



# Micelle-bound structures and dynamics of the hinge deleted analog of melittin and its diastereomer: Implications in cell selective lysis by D-amino acid containing antimicrobial peptides

Rathi Saravanan, Anirban Bhunia, Surajit Bhattacharjya \*

Biomolecular NMR and Drug Discovery Laboratory, School of Biological Sciences, Division of Structural and Computational Biology, Nanyang Technological University, Singapore 637551, Singapore

## ARTICLE INFO

### Article history:

Received 14 April 2009

Received in revised form 4 June 2009

Accepted 17 July 2009

Available online 25 July 2009

### Keywords:

Melittin  
Antimicrobial peptide  
AMPs  
Helical AMPs  
Antibiotic resistance

## ABSTRACT

Melittin, the major component of the honey bee venom, is a 26-residue hemolytic and membrane active peptide. Structures of melittin determined either in lipid environments by NMR or by use of X-ray demonstrated two helical regions at the N- and C-termini connected by a hinge or a bend at the middle. Here, we show that deletion of the hinge residues along with two C-terminal terminal Gln residues (Q25 and Q26), yielding a peptide analog of 19-residue or Mel-H, did not affect antibacterial activity but resulted in a somewhat reduced hemolytic activity. A diastereomer of Mel-H or Mel-<sup>d</sup>H containing D-amino acids [<sup>d</sup>V5, <sup>d</sup>V8, <sup>d</sup>L11 and <sup>d</sup>K16] showed further reduction in hemolytic activity without lowering antibacterial activity. We have carried out NMR structures, dynamics (H–D exchange and proton relaxation), membrane localization by spin labeled lipids, pulse-field-gradient (PFG) NMR and isothermal titration calorimetry (ITC) in dodecylphosphocholine (DPC) micelles, as a mimic of eukaryotic membrane, to gain insights into cell selectivity of these melittin analogs. PFG-NMR showed Mel-H and Mel-<sup>d</sup>H both were similarly partitioned into DPC micelles. ITC demonstrated that Mel-H and Mel-<sup>d</sup>H interact with DPC with similar affinity. The micelle-bound structure of Mel-H delineated a straight helical conformation, whereas Mel-<sup>d</sup>H showed multiple β-turns at the N-terminus and a short helix at the C-terminus. The backbone amide-proton exchange with solvent D<sub>2</sub>O demonstrated a large difference in dynamics between Mel-H and Mel-<sup>d</sup>H, whereby almost all backbone protons of Mel-<sup>d</sup>H showed a much faster rate of exchange as compared to Mel-H. Proton T<sub>1</sub> relaxation had suggested a mobile backbone of Mel-<sup>d</sup>H peptide in DPC micelles. Resonance perturbation by paramagnetic lipids indicated that Mel-H inserted deeper into DPC micelles, whereas Mel-<sup>d</sup>H is largely located at the surface of the micelle. Taken together, results presented in this study demonstrated that the poor hemolytic activity of the D-amino acid containing analogs of antimicrobial peptides may be correlated with their flexible dynamics at the membrane surface.

© 2009 Elsevier B.V. All rights reserved.

## 1. Introduction

Linear alpha helical antimicrobial peptides (AMPs) are abundantly present, over 150 in AMSDb database, in all life forms [1–7]. These peptides are usually short (<40 residues) and rich in non-polar and cationic amino acids. Although in free solution, they exist in largely unstructured conformations, however, upon interactions with lipids or in the presence of organic co-solvents amphipathic helical structures are readily stabilized [8–12]. As a mode of their action, this class of peptides efficiently permeabilizes both the outer and inner membranes of the microorganisms following one or more types of mechanisms e.g. barrel stave, toroidal pore, or carpeting the target cells [13–15]. Structure–activity relationship (SAR) studies have been

extensively carried out for helical antimicrobial peptides to understand mechanism of cell lysis, to improve broad spectrum property and elimination of cyto-toxicity [2,12,16–18]. Sequence modifications studies suggested that cell selectivity of the helical AMPs may involve several parameters including hydrophobicity, amphipathicity and structuring in lipid membranes [2,12]. Although, a consensus of ideal parameters appeared to be difficult to deduce, however, a high ratio of hydrophobic to cationic residues tends to decrease cell selective property of antimicrobial peptides [2,12].

Melittin, a major component of the venom of European honey bee, is a 26-residue membrane active peptide [19]. Melittin is highly cytolytic, causes efficient lysis of red blood cells at a very low concentration and also possesses antibacterial activities towards Gram negative and Gram positive bacteria [20,21]. Therefore, the dissociation of hemolytic and antibacterial activities would be desirable to obtain melittin based antimicrobials. Interactions of native melittin with various types of lipid membranes have been extensively inves-

\* Corresponding author. Fax: +65 6791 3856.

E-mail address: [surajit@ntu.edu.sg](mailto:surajit@ntu.edu.sg) (S. Bhattacharjya).



**Table 1**  
Antimicrobial and hemolytic activities of Mel-H and Mel-<sup>d</sup>H.

Peptides	MIC ( $\mu\text{M}$ )			Hemolytic activity (%)	
	<i>E. coli</i>	<i>P. aeruginosa</i> (ATCC27853)	<i>S. aureus</i> (ATCC25923)	0.4 $\mu\text{M}$	23 $\mu\text{M}$
Mel-H	11.25	11.25	5.6	28	42
Mel- <sup>d</sup> H	12.50	12.50	6.2	5	12
Melittin	11.25	11.25	5.6	100	100

showed drastic differences in dynamics and micellar localizations. Whereby, Mel-<sup>d</sup>H has demonstrated a surface localization with a higher mobility in DPC micelles. Our results shed novel mechanistic insights into the plausible roles of structures and dynamics that may be important for explaining basis of cell selective interactions by diastereomeric antimicrobial peptides.

## 2. Materials and methods

### 2.1. Peptide synthesis, melittin and lipids

Crude Mel-H and Mel-<sup>d</sup>H, peptides were purchased from GL Biochem (Shanghai) Ltd and purified by reverse phase HPLC. Melittin and DPC were obtained from Sigma and Avanti Polar Lipids, respectively. Deuterated DPC- $d_{38}$  was purchased from Cambridge Isotope Laboratories (CIL, Inc.).

### 2.2. Hemolytic assay

Fresh human red blood cells (hRBCs) were washed thrice with 10 mM PBS (phosphate buffer saline), at pH 7.4 by centrifugation for 10 min at 800 g and resuspended into PBS to a final concentration of

$1 \times 10^9$  erythrocytes/ml. Equal volume of erythrocytes were incubated with varied concentrations of the peptides with shaking for 1 h. Samples were centrifuged at 900 g for 15 min at 4 °C. The RBC lysis and release of hemoglobin as a function of concentrations of peptides were measured at an optical density of 540 nm. The maximal (100%) hemolysis was determined using 2% Triton X-100 as a control. Percentage of hemolytic activity of the peptides was calculated relative to Triton X-100 sample [53].

### 2.3. Antibacterial assay

The antimicrobial activities of the analog peptides and melittin were analyzed with Gram negative *Escherichia coli*, *Pseudomonas aeruginosa* (ATCC 27853) and Gram positive *Staphylococcus aureus* (ATCC 25923) strains. Mid-log phase bacterial cells obtained from an overnight culture were washed thrice with 10 mM sodium phosphate buffer, at pH 7.4 by centrifugation at 4000 r.p.m for 10 min at 4 °C. The resuspended pellet was diluted to an optical density of 0.2 at 600 nm. In a 96-well microtiter plate equal volumes (50  $\mu\text{l}$ ) of the corresponding bacterial strains were incubated with serially diluted peptides for 3 h at 37 °C. The incubated bacteria were then streaked on to Muller Hilton agar plates. The lowest concentration at which the peptide inhibited complete growth of the bacteria was taken as the MIC value of the peptide for the corresponding bacterial strains.

### 2.4. Isothermal titration calorimetry (ITC) studies

All ITC experiments were performed on VP-ITC calorimeter (Micro Cal Inc, Northampton, MA) at 30 °C. Peptide and DPC micelles were dissolved in water at pH 6.0. DPC micelles were loaded into the syringe. The reference cell was filled with unbuffered water at same pH. Titrations were performed with addition of 5  $\mu\text{l}$  aliquots of

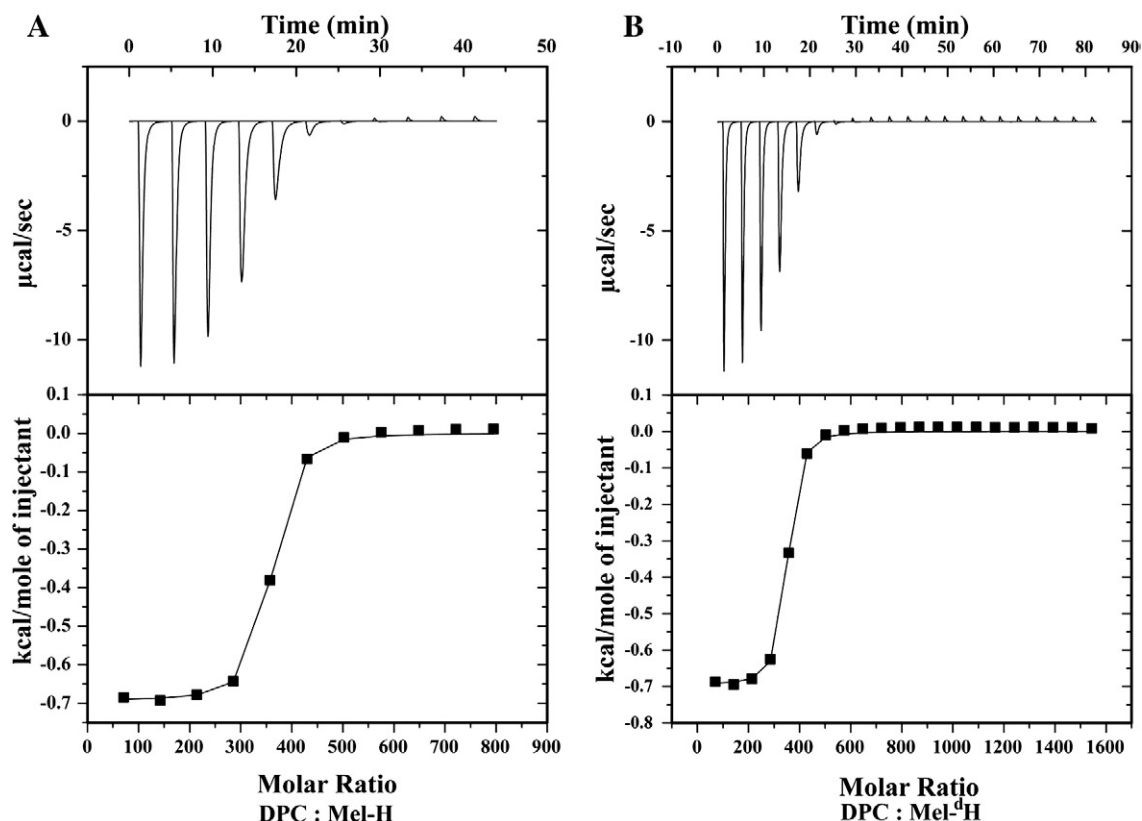


**Fig. 2.** Thermodynamics of interaction between Mel-H (in panel A) and Mel-<sup>d</sup>H (panel B) with DPC micelles. ITC traces were obtained by titrating 5  $\mu\text{l}$  aliquots of 100 mM DPC into either 5  $\mu\text{M}$  Mel-H or Mel-<sup>d</sup>H peptides kept in the sample cell in water pH 6 at 30 °C. Typically twenty injections of lipid were performed at an interval of 4 min and the reaction cell was constantly stirred at 300 r.p.m. Plots of heats of reaction as a function of either Mel-H/DPC or Mel-<sup>d</sup>H/DPC molar ratio were obtained using a non-linear least square fit.

100 mM DPC into sample cell containing 5  $\mu$ M of either Mel-H or Mel-<sup>d</sup>H. The reaction cell was constantly stirred at 300 r.p.m and the heat exchange was recorded. The resulting data were integrated with Micro Cal Origin 5.0 after correction for the heat of dilutions. A single site binding model provided with software was fitted to the data by a non-linear least square analysis yielding equilibrium association constant ( $K_a$ ) and the enthalpy change,  $\Delta H$ . The Gibb's free energy change  $\Delta G$  and entropy change  $\Delta S$  were calculated from the fundamental thermodynamic equations  $\Delta G = -RT \ln K_a$  and  $\Delta S = (\Delta H - \Delta G)/T$ , respectively.

### 2.5. NMR experiments

All NMR experiments were performed on a Bruker DRX 600 MHz spectrometer, equipped with a cryoprobe. For structure determination of Mel-H and Mel-<sup>d</sup>H, 0.5 mM of the peptides at pH 3.2 were used. For DPC- $d_{38}$  (200 mM) micelle-bound structure determination, 2-D <sup>1</sup>H-<sup>1</sup>H TOCSY (mixing time = 80 ms), 2-D <sup>1</sup>H-<sup>1</sup>H NOESY (mixing time = 200 ms) and <sup>13</sup>C-HSQC (natural abundance) of both Mel-H and Mel-<sup>d</sup>H at 310 K, were performed. Hydrogen deuterium exchange experiments were carried out by acquiring a series of 2-D <sup>1</sup>H-<sup>1</sup>H TOCSY (mixing time = 80 ms) with 90 min interval at 310 K. The lyophilized samples of peptide and DPC micelle were directly dissolved in 100% D<sub>2</sub>O and TOCSY spectra were collected as a function of time. Paramagnetic Relaxation Enhancement (PRE) experiments were performed by addition of aliquots of either of 5-doxyl-stearic acid (5-DSA) or 16-doxyl-stearic acid (16-DSA) dissolved in deuterated methanol into sample containing micelle-bound peptides. NMR experimental parameters were kept constant for all the measurements except for the changes in probe tuning and field shimming. The intensities of the cross peaks were measured before and after the addition of the paramagnetic probes. The results were plotted in terms of Remaining amplitude (RA) =  $A(\text{probe})/A(0)$ , where  $A(\text{probe})$  and  $A(0)$  are the intensity of the cross peaks after and before the addition of probe, respectively [54]. The proton longitudinal relaxation ( $T_1$ ) measurements of the micelle-bound peptides were measured with relaxation delays of 5 ms, 40 ms, 80 ms, 130 ms, 210 ms, 330 ms, 470 ms, 630 ms, 800 ms and 1000 ms.  $T_1$  values were determined by fitting the signal intensities to a single exponential function. The hydrodynamic radii of the micelle-bound Mel-H and Mel-<sup>d</sup>H were determined using pulse-field-gradient NMR method with PG-SLED pulse sequence at 310 K. Native melittin peptide dissolved in 200 mM DPC- $d_{38}$  micelle was used as a control. A series of 1-D proton NMR spectra with incremented gradient strength from 2 to 95% was acquired. The proton signal decay was then fitted to a single Gaussian expression:  $I(g) = Ae^{-dg^2}$ , where  $I$ ,  $g$ , and  $d$  represent intensity of the signals, gradient strengths and decay rates, respectively. The hydrodynamic radius was calculated using the equation  $R_h = d_{\text{ref}}/d \times R_{h,\text{ref}}$  where  $R_h$  is the hydrodynamic radius of the peptide/DPC micelle complex,  $d_{\text{ref}}$  and  $d$  are the decay rate of the reference molecule, CH<sub>3</sub>COO<sup>-</sup> and peptide/DPC micelle complex, respectively. The hydrodynamic radius of CH<sub>3</sub>COO<sup>-</sup> was taken as 2.3 Å [55].

### 2.6. NMR derived structure calculations

Structure calculations were carried out using the DYANA program [56]. Inter-proton distances for the peptide-DPC micelle-bound structure were obtained from the 2-D <sup>1</sup>H-<sup>1</sup>H NOESY spectra. NOESY peaks were categorized as strong, medium and weak based on the signal intensity and were translated into distance constraints as 2.5 Å, 3.5 Å and 5.0 Å, respectively. Additionally, dihedral angle restraints were obtained from TALOS [57] using C<sup>α</sup> and H<sup>α</sup> chemical shifts and were used for structure calculation with  $\pm 25^\circ$  variation from the calculated dihedral values. Several rounds of structure calculations were performed. Depending on the NOE violations the angle and distance

**Table 2**

Thermodynamic parameters obtained for Mel-H and Mel-<sup>d</sup>H interactions with DPC micelles in water at pH 6, 30 °C.

Peptide	$K_a$ (M <sup>-1</sup> )	$\Delta H$ (kcal/mol)	$\Delta G$ (kcal/mol)	$T\Delta S$ (kcal/mol)
Mel-M	$49.9 \times 10^6$	-8.0	-10.7	2.7
Mel-D	$43.5 \times 10^6$	-6.0	-10.6	4.6

constraints were adjusted. 100 structures were calculated and only 20 lowest energy conformers were selected for the NMR ensemble.

## 3. Results

### 3.1. Design of hinge deleted analog of melittin

Three-dimensional structures of melittin determined either by X-ray or NMR had indicated that molecule adopts helical structure with a bend ( $\sim 120^\circ$ ) at the middle. A stretch of residues T10-P14 (Fig. 1) is found to be involved in stabilizing a curved or kinked geometry of melittin. Crystal structure of melittin shows non-helical hydrogen bonding pattern in this segment e.g. amide nitrogen of residue L13 is hydrogen bonded to carbonyl oxygen of residue V8 ( $i$  to  $i + 5$ ) and carbonyl oxygen residue T10 cannot form hydrogen bond with P14 [43]. Furthermore, backbone dihedral angles ( $\phi$ ,  $\psi$ ) of residues T11 and G12 showed significant deviations from an ideal helical

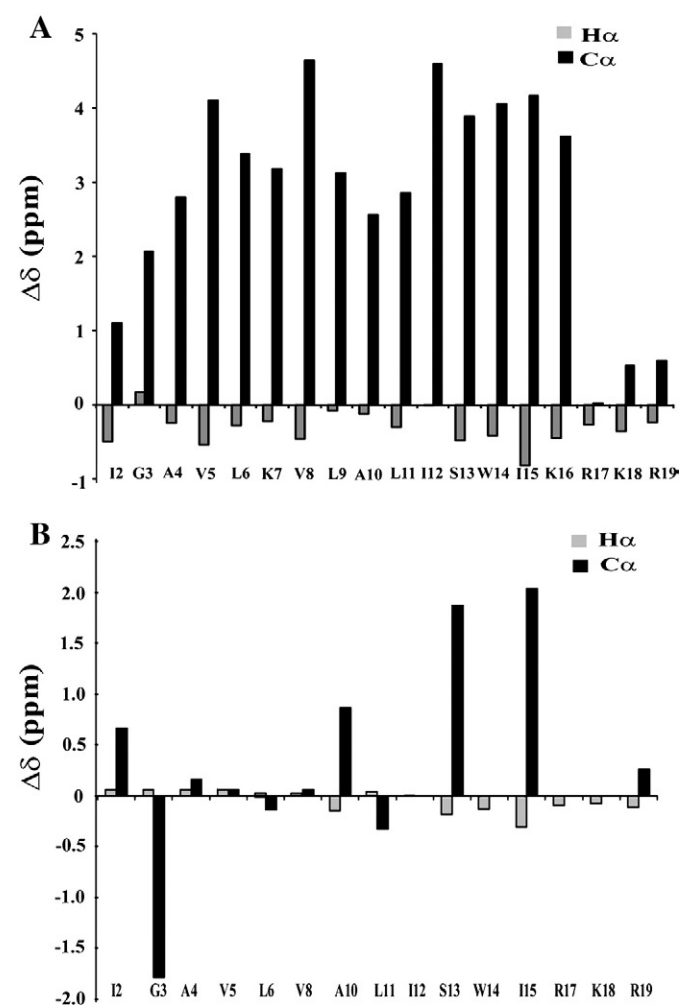


**Fig. 3.** Chemical shift deviations from random coil values for C<sup>α</sup>H (in light grey bars) and <sup>13</sup>C<sup>α</sup> (in black bars) resonances of Mel-H (in panel A) and Mel-<sup>d</sup>H (in panel B) bound to deuterated DPC micelles.

conformation [43]. We have prepared a deleted analog of melittin, Mel-H, lacking these residues T10–P14 (Fig. 1A). In order to shorten the peptide, the last two Gln residues are also removed. Since, previous studies demonstrated that these residues are not essential for antimicrobial or hemolytic activities of melittin [28]. We have also synthesized a diastereomer of Mel-H containing D-amino acid at  $^dV5$ ,  $^dV8$ ,  $^dL11$  and  $^dK16$  positions (Fig. 1A). In comparison to melittin, Mel-H contains, based on the sequence, a higher hydrophobicity and a lower hydrophobic moment or amphipathicity (Fig. 1A). Fig. 1B represents the helical wheel projections of melittin and Mel-H comparing distribution of residues with the removal of hinge. The hydrophobicity of the diastereomer of Mel-H or Mel- $^dH$  appears to be slightly higher than Mel-H as suggested by a longer retention time in HPLC column (Fig. 1A).

### 3.2. Antibacterial and hemolytic activities of the analogs

The antimicrobial activities of melittin, Mel-H and Mel- $^dH$  were analyzed against Gram negative bacterial strains *E. coli*, *P. aeruginosa* (ATCC 27853) and Gram positive strain *S. aureus* (ATCC 25923)

(Table 1). The MIC values determined for melittin are in agreement with previous reports [29]. Mel-H demonstrated high antimicrobial activities against *E. coli*, *P. aeruginosa* and *S. aureus*, akin to native melittin (Table 1). The diastereomeric analog, Mel- $^dH$ , also exhibited potent antimicrobial activities against all three organisms (Table 1). Experiments were repeated three times and similar results were observed. These data suggest that the removal of hinge residues from melittin sequence and further incorporation of D-amino acids have no significant effects in the antimicrobial activities. By contrast, the hemolytic activity of the Mel- $^dH$  peptide is found to be significantly lower as compared to melittin and Mel-H (Table 1). The Mel-H peptide showed >42% hemolysis at a peptide concentration of 23  $\mu\text{M}$ , which is higher than its MIC values (Table 1). Previously, a melittin diastereomer containing D-amino acids at  $^dV5$ ,  $^dV8$ ,  $^dI17$ , and  $^dK23$  positions had shown reduction in hemolytic activity [37]. Taken together, these functional studies demonstrate that the hinge region of melittin is not indispensable for antimicrobial activities. The hemolytic activity of Mel-H, observed at higher concentrations, suggests that residues involved in bent formation in

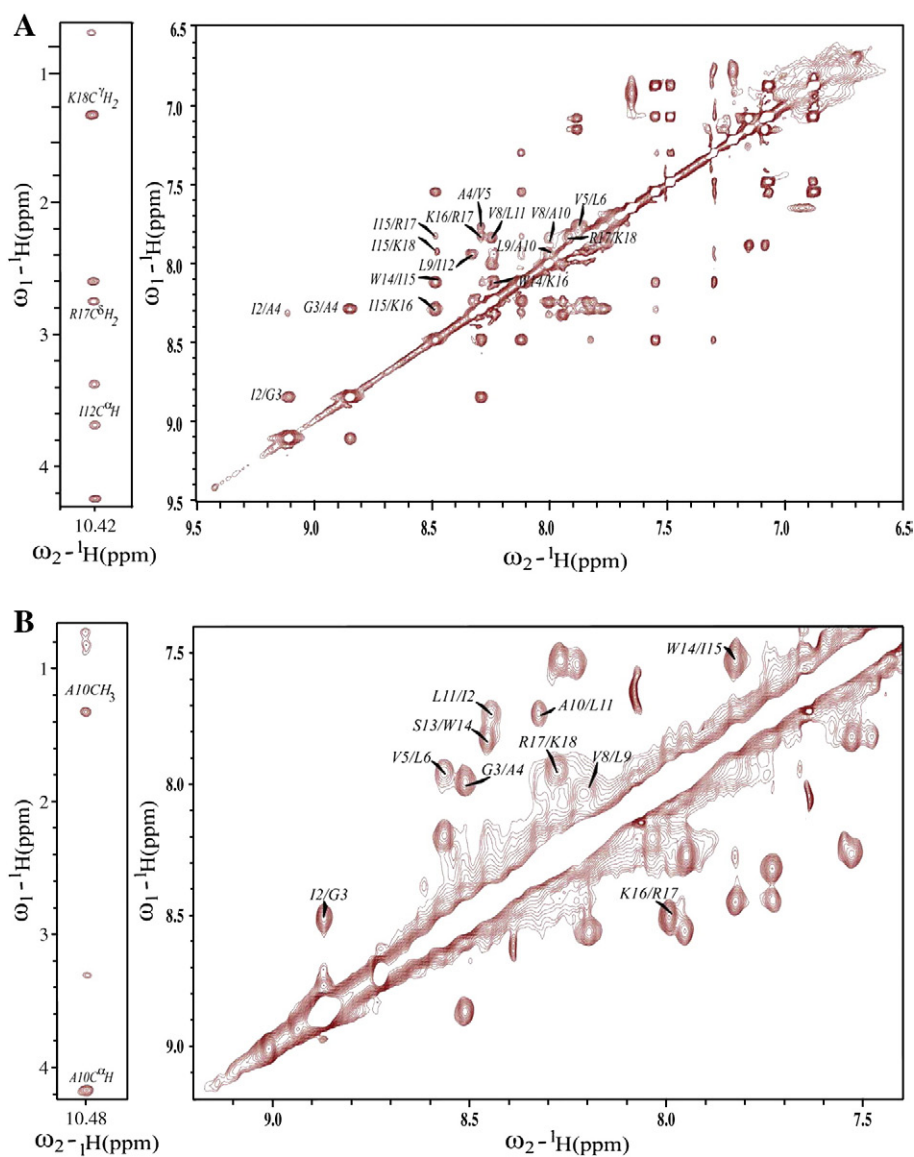


**Fig. 4.** (panel A) Sections of two-dimensional  $^1\text{H}$ - $^1\text{H}$  NOESY spectra of Mel-H showing NOE contacts from the downfield shifted indole  $\text{N}^{\text{H}}$  of W14 with aliphatic resonances (panel A, left) and NOEs involving backbone amide protons (panel A, right). (panel B) Sections of two-dimensional NOESY spectra of Mel- $^dH$  showing NOE contacts from the downfield shifted indole  $\text{N}^{\text{H}}$  of W14 with aliphatic resonances (panel B, left) and NOEs involving backbone amide protons (panel B, right). The NOESY experiments were carried out in 200 mM DPC- $d_{38}$ , 0.5 mM peptides in aqueous solution, at 310 K.

melittin helix have potential roles in augmenting hemolytic activity of the peptide. On the other hand, an extremely poor hemolytic activity and potent antimicrobial activities of the Mel-<sup>d</sup>H peptide, further considering its shorter length, may be exploited for therapeutic applications.

### 3.3. Partitioning and binding affinities of the Mel-H and Mel-<sup>d</sup>H to DPC micelles

The low hemolytic activity of Mel-<sup>d</sup>H may potentially arise from its reduced intrinsic affinity to the zwitterionic lipids. The binding affinity and incorporation into DPC micelles of the Mel-H and Mel-<sup>d</sup>H were thereby investigated by ITC and PFG-NMR methods, respectively. Fig. 2 shows ITC thermograms and corresponding titration curves for Mel-H and Mel-<sup>d</sup>H peptides. The binding and thermodynamic parameters are listed in Table 2. Clearly, both peptides demonstrate binding induced exothermic heat release as they form complex with DPC micelles (Fig. 2). The DPC/peptide binding interactions appeared to be driven by favorable changes in enthalpy, as indicated by the downward trend of the ITC peaks (Fig. 2, top panels) and resultant negative integrated heats (Fig. 2, bottom panels). The equilibrium association constants ( $K_a$ ) and thermodynamic parameters of Mel-M and Mel-<sup>d</sup>H (Table 2) revealed that they have very similar binding affinity toward DPC micelles.

We have determined hydrodynamic radii of the DPC-d<sub>38</sub>/peptide complexes by PFG-NMR by monitoring decay of peptide resonances as a function of gradient strength (see Materials and methods). The peptide with lower partitioning into DPC micelles is expected to exhibit a faster decay of NMR signals. Interestingly, both Mel-H and Mel-<sup>d</sup>H demonstrated similar decay pattern of NMR signals in these experiments (Supplementary Figure S1), indicating a very similar incorporation into DPC micelles. The hydrodynamic radii of the DPC/Mel-H and DPC/Mel-<sup>d</sup>H complexes are found to be 25.61 Å and 25.54 Å, respectively. These data suggest that both peptides are stably held with the DPC micelles.

### 3.4. NMR studies of Mel-H and Mel-<sup>d</sup>H in DPC micelle

Comparison of one-dimensional proton NMR spectra of Mel-H and Mel-<sup>d</sup>H, in the free and in presence of 200 mM DPC-d<sub>38</sub>, showed a large dispersion in chemical shifts in micelle-bound states, indicating both peptides exist in complex with micelles. Sequence-specific proton resonance assignments were obtained by combined use of two-dimensional TOCSY and NOESY spectra [58]. The deviation of C<sup>α</sup>H and <sup>13</sup>C<sup>α</sup> chemical shifts from random coil values is a reliable indicator of secondary structures [59]. A continuous helical structure, residue I2-R19, for Mel-H can be deduced from the chemical shift deviations (Fig. 3A), as indicated by the upfield shifts of C<sup>α</sup>H and the downfield shifts of <sup>13</sup>C<sup>α</sup> resonances from random coil. By contrast, the helical structure for Mel-<sup>d</sup>H appeared to be perturbed, restricted only to the C-terminus residues S13-R19, due to the incorporation of D-amino acids (Fig. 3B). The presence of a number of high intensity sequential NH/HN and medium range C<sup>α</sup>H/NH (i to i + 3) and (i to i + 4) NOEs typical of α helical structure can be identified along the entire stretch of Mel-H, suggesting formation of a continuous helical structure (Figs. 4A and 5A). Several sidechain/sidechain or backbone/sidechain NOEs are also observed for Mel-H including NOEs between A4-K7, W14-K18, A10-W14 and L11-I15. Notably, the indole proton of W14 shows NOE contacts with sidechain protons of Lys18 (Fig. 4A, left panel). These sidechain/sidechain NOEs involving residues W19 and K23, were also observed in the native melittin in DPC micelles [44].

By contrast, the NOESY spectra of Mel-<sup>d</sup>H in DPC micelle had relatively lower number of NOE crosspeaks. The C-terminus of the molecule showed sequential NH/NH NOEs and medium range C<sup>α</sup>H/NH (i to +i + 3) and (i to i + 4) NOEs (Figs. 4B and 5B),

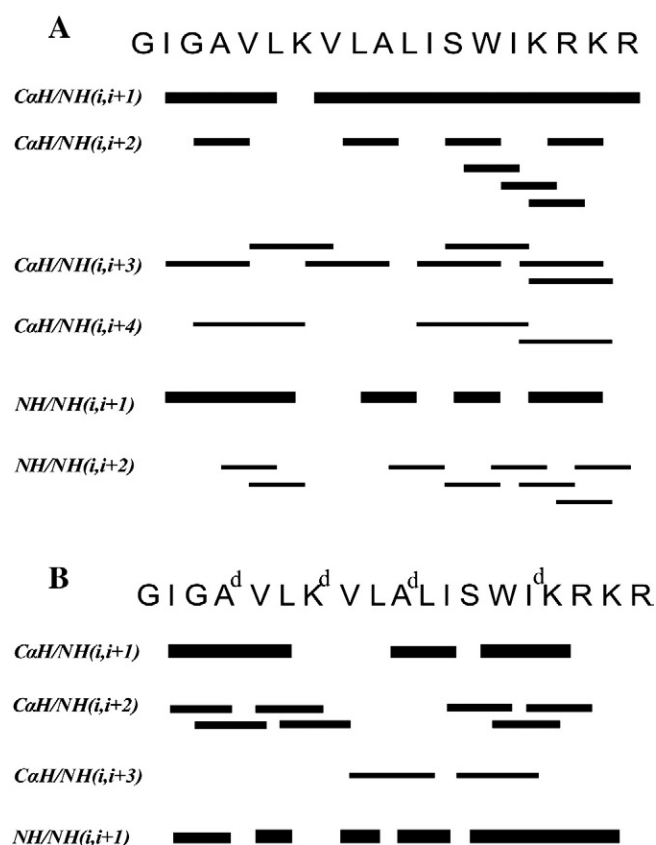


Fig. 5. Bar diagram summarizing the sequential and medium range NOE's observed for deuterated DPC micelle-bound Mel-H (panel A) and (B) Mel-<sup>d</sup>H (panel B) obtained from two-dimensional <sup>1</sup>H-<sup>1</sup>H NOESY spectrum. The thickness of the bar corresponds to the relative intensities of NOE cross-peak. Amino acid sequences of Mel-H and Mel-<sup>d</sup>H are shown at the top.

indicating a helical conformation for these residues. On the other hand, at the N-terminus, there were sequential HN/HN NOEs and few C<sup>α</sup>H/NH (i to i + 2) NOEs (Figs. 4B and 5B). The NOEs between indole ring proton of W14 and K18 were not detected (Fig. 4B, left panel).

### 3.5. Three-dimensional structures of Mel-H and Mel-<sup>d</sup>H in DPC micelle

An ensemble of 20 structures for Mel-H and Mel-<sup>d</sup>H in DPC were calculated using DYANA (see Materials and methods). The superposition of the backbone atoms (C<sup>α</sup>, C' and N) of the 20 lowest energy structures of Mel-H and Mel-<sup>d</sup>H revealed that both peptides adopt a defined structure in DPC micelles (Fig. 6). However, Mel-H has a lower RMSD values for the backbone and all heavy atoms (Table 3). The backbone dihedral angles ( $\Phi$ ,  $\Psi$ ) were clustered at the most favored regions at the Ramachandran plot for all the residues in Mel-H and in Mel-<sup>d</sup>H (Table 3).

DPC-bound structure of Mel-H is determined by a straight alpha helix encompassing residues I2-I15 (Fig. 7A). One face of the helix is highly hydrophobic consisted of residues I2, V5, L6, V8, L9, I12 and I15 (Fig. 7A). The opposite face of Mel-H helix contains cationic residues, K7, R17, K18 and aromatic residue W14, providing an amphipathic property of the helix (Fig. 7A). The aromatic ring of W14 showed a cation- $\pi$  type packing interaction with residue K18 (Fig. 7A). The continuity of hydrophilic or cationic face of the helix appears to be disrupted by the packing of non-polar residues L6, A10 and L11 (Fig. 7A).

Solution structure of the Mel-<sup>d</sup>H peptide in complex with DPC micelles showed multiple turns at the N-terminus presumably nucleated by the D-amino acids (Fig. 7B). In these multiple turn

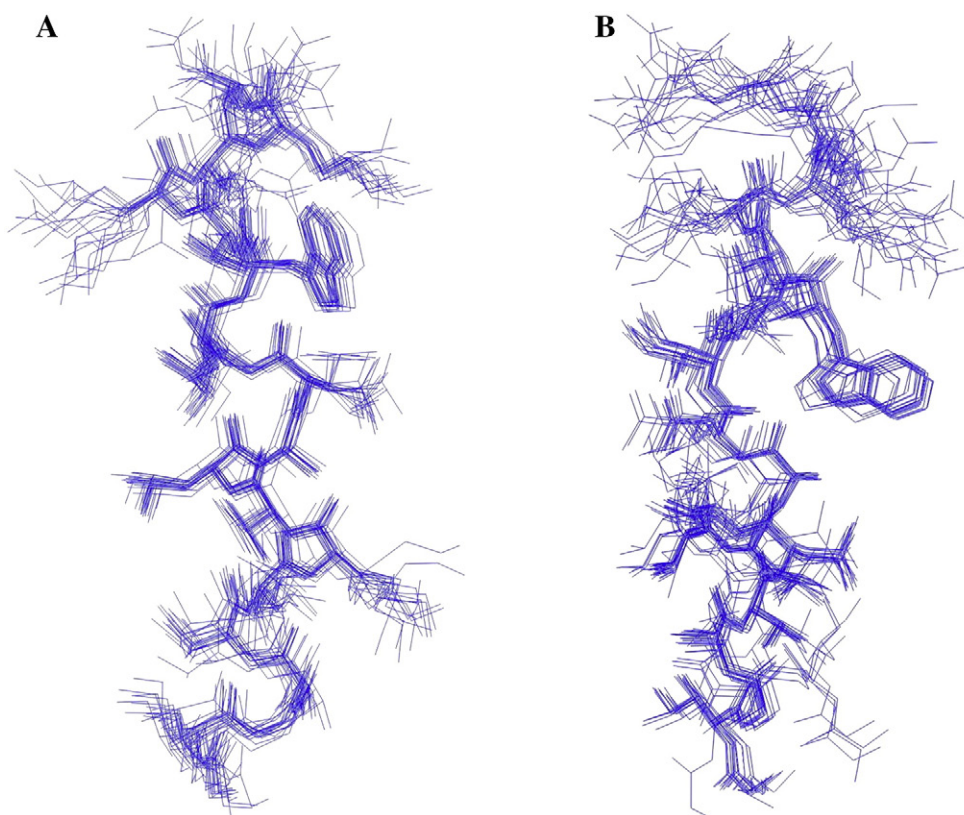


**Fig. 6.** Superposition of the 20 lowest energy structures of Mel-H (panel A) and Mel-<sup>d</sup>H (panel B) peptides bound to DPC micelles obtained from distance geometry calculations using TALOS predicted dihedral angles and DYANA program.

conformations, the amide protons of the residues <sup>d</sup>V5, <sup>d</sup>V8 and <sup>d</sup>L11 are found to be involved in the plausible hydrogen bond formations with C=O of residues I2, <sup>d</sup>V5 and <sup>d</sup>V8 (Fig. 7C), respectively. In H–D exchange studies of Mel-<sup>d</sup>H these amide protons including few others from the C-terminus helical region were found to be protected from immediate exchange with solvent (*vide infra*). Interestingly, despite the lack of a continuous helical structure of Mel-<sup>d</sup>H, the sidechains are found to be oriented into an amphipathic manner (Fig. 7B), whereby non-polar residues I2, <sup>d</sup>V5, <sup>d</sup>V8, <sup>d</sup>L11, I12 and I15 are segregated into one side of the structure. Despite the absence of NOE contacts, the aromatic ring of W14 has been found to be in same region with residue K18 (Fig. 7B).

**Table 3**

Summary of the structural statistics of Mel-H and Mel-<sup>d</sup>H in deuterated DPC micelles.

	Mel-H	Mel- <sup>d</sup> H
Distance restraints		
Total	127	98
Intra-residue ( $i - j = 0$ )	60	41
Sequential ( $ i - j  = 1$ )	37	38
Medium-range ( $2 \leq  i - j  \leq 4$ )	19	0
Long-range ( $ i - j  \geq 5$ )	0	0
Angular restraints ( $\Phi, \Psi$ )	18	18
Distance restraints violations		
Number of violations	6	6
Average violation	$\leq 0.26$ Å	$\leq 0.35$ Å
Maximum violation	$\leq 0.26$ Å	$\leq 0.38$ Å
Deviation from mean structure (for all residues)		
Backbone ( $C^\alpha, C'$ , and N)	$0.30 \pm 0.17$ Å	$0.81 \pm 0.52$ Å
Heavy atoms	$0.94 \pm 0.21$ Å	$1.37 \pm 0.49$ Å
Ramachandran plot for the mean structure		
% residues in the most favorable and additionally allowed region	100%	93.8%
% residues in the generously allowed region	0%	6.2%
% residues in the disallowed region	0%	0%

### 3.6. Localization of Mel-H and Mel-<sup>d</sup>H in DPC micelles

The depth of insertion of Mel-M and Mel-<sup>d</sup>H into DPC micelles were investigated by two nitro-oxide paramagnetic probes 5-doxyl-stearic acid (5-DSA) and 16-doxyl-stearic acid (16-DSA). 5-DSA with the paramagnetic doxyl moiety at the fifth position affects those residues that are located close to surface, while 16-DSA with the spin label at the sixteenth carbon position perturb those residues which are deeply inserted in the lipid micelle [49]. Perturbations were expressed as a ratio of remaining amplitude (RA) in the presence of 5-DSA and 16-DSA lipids (Fig. 8). Interestingly, residues I2–I15 of Mel-H show significant perturbations (>50%) by 16-DSA, indicating these residues may be inserted into the non-polar region of micelles (Fig. 8A). On the other hand, the four positively charged residues, KRKR, at the C-terminus of Mel-H could be located at the micelles surface as these residues are largely affected only by 5-DSA (Fig. 8A). The resonance perturbations induced by the paramagnetic probes for Mel-<sup>d</sup>H can be obtained for all but residues K7, L9, A10 and K16 as a result of resonance overlap (Fig. 8B). Significant resonances perturbations by both the lipids can be seen indicating Mel-<sup>d</sup>H is also inserted into DPC micelles (Fig. 8B). Interestingly, residues <sup>d</sup>V5, L6, <sup>d</sup>V8, <sup>d</sup>L11 and I12 demonstrate a more reduction in signal intensities, indicating a deeper localization of these non-polar residues into the micelles (Fig. 8B). A comparative analysis of resonance perturbation of the two peptides by the paramagnetic lipids indicates that 16-DSA is an effective quencher against Mel-H, whereas 5-DSA appears to have a more pronounced effect for the diastereomer, Mel-<sup>d</sup>H (Fig. 8C). A larger perturbation of the hydrophobic residues at the N-terminus of Mel-H, as compare to the positively charged C-terminus, indicates that the N-terminus of the peptide may be located inside the hydrophobic core of micelles. Taken together, we propose that Mel-H might adopt a perpendicular or an oblique orientation, rather than a

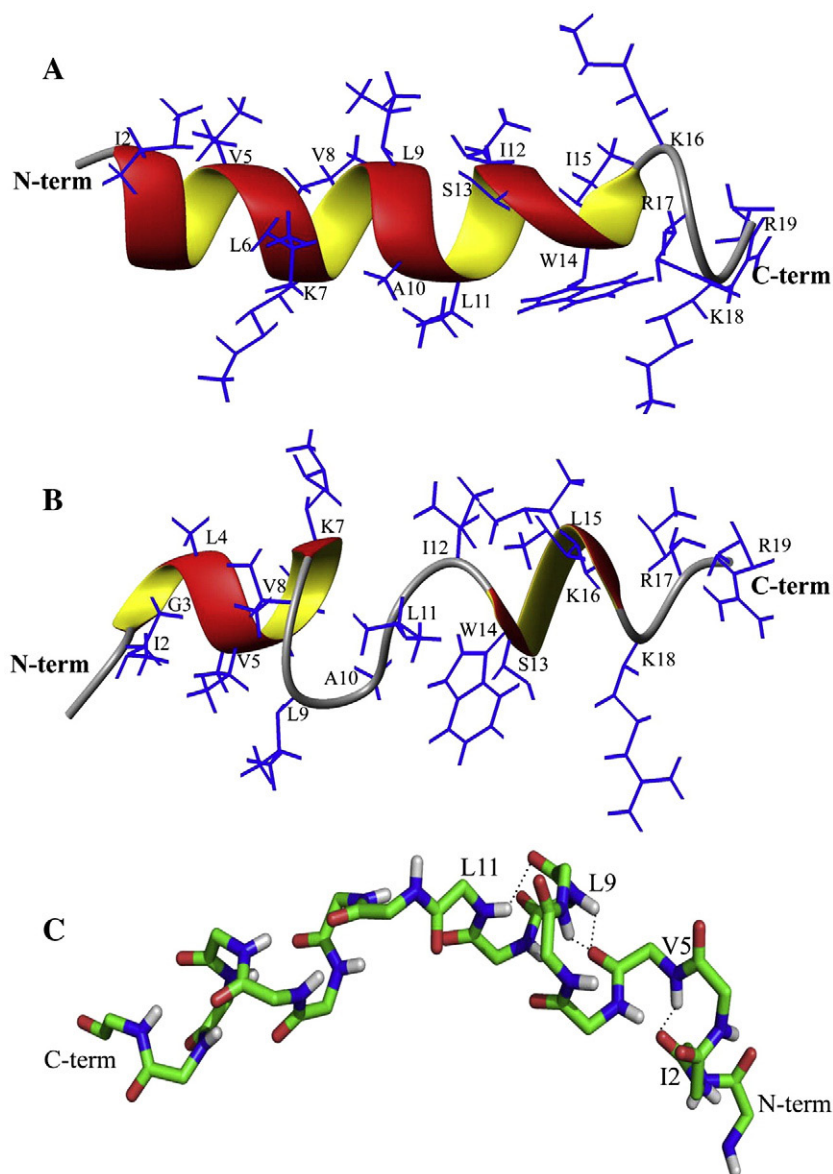


**Fig. 7.** Ribbon representation of the average DPC-bound NMR structures of Mel-H (panel A) and Mel-dH (panel B) showing disposition of the sidechain contacts. (panel C) A stick representation of the backbone structure of Mel-dH indicating plausible hydrogen bonds between residues I2 C=O to V5 H-N, V5 C=O to H-N V8, V5 C=O to H-N L9 and L9 C=O-H-N L11 stabilizing the multiple turn conformations at the N-terminus of Mel-dH in DPC-bound state.

parallel one, in DPC micelles. In case of Mel-dH although there was perturbation by the both probes, presumably owing to the fast dynamics of the peptide (see below), perturbation by 5-DSA was more evident, indicating a plausible parallel orientation for Mel-dH in DPC micelles (Fig. 8C).

### 3.7. H-D exchange and longitudinal relaxation ( $T_1$ ) studies of Mel-H and Mel-dH in DPC micelles

Backbone amide-proton exchange rates of micelle-bound peptides are plausible indicators of the stability of peptide/micelle complex. Dynamics of Mel-H and Mel-dH in DPC micelles were examined by H-D exchange studies and  $T_1$  relaxation measurements. Freshly dissolved samples of Mel-H and Mel-dH showed a number of amide protons those are protected against the exchange (Fig. 9, panels A and C). However, most of these amide protons are found to be rapidly exchanged with solvent D<sub>2</sub>O in case of Mel-dH peptide (Fig. 9D). Low intense C<sup>α</sup>H/HN peaks in the TOCSY spectra were observed for residues <sup>d</sup>V5, <sup>d</sup>V8, <sup>d</sup>L11 and I15 after 90 min of

exchange (Fig. 9D). There were no amide-proton signals of Mel-dH after 180 min of exchange period (data not shown). On the other hand, the amide protons of Mel-H including residues I2, G3, V5, L6, K7, V8, L9, A10, L11, I12, W14 and I15 demonstrate a slow exchange against the solvent (Fig. 9B). The amide protons of residues W14 and I15 were visible even after 12 h of exchange. These results indicate that in complex with the zwitterionic DPC micelles DPC Mel-H has a less conformational flexibility as compared to its diastereomer, Mel-dH.

To further analyze the large difference in the H-D exchange of the micelle-bound peptides, proton  $T_1$  relaxation experiments were performed. Relaxation measurements ( $T_1$  and  $T_2$ ) are excellent indicators of dynamics of molecules. In these measurements, one would expect higher  $T_1$  values for residues undergoing large scale dynamics. The  $T_1$  value, 0.5 s, for the residue L11 sidechain methyl groups, of Mel-H peptide was found to be lower as compared to that of Mel-dH, 0.72 s, in micelle-bound states (Fig. 10).  $T_1$  values were also lowered for the aromatic ring protons of residue W14 in Mel-H, indicating its less conformational flexibility. The high  $T_1$  of Mel-dH in

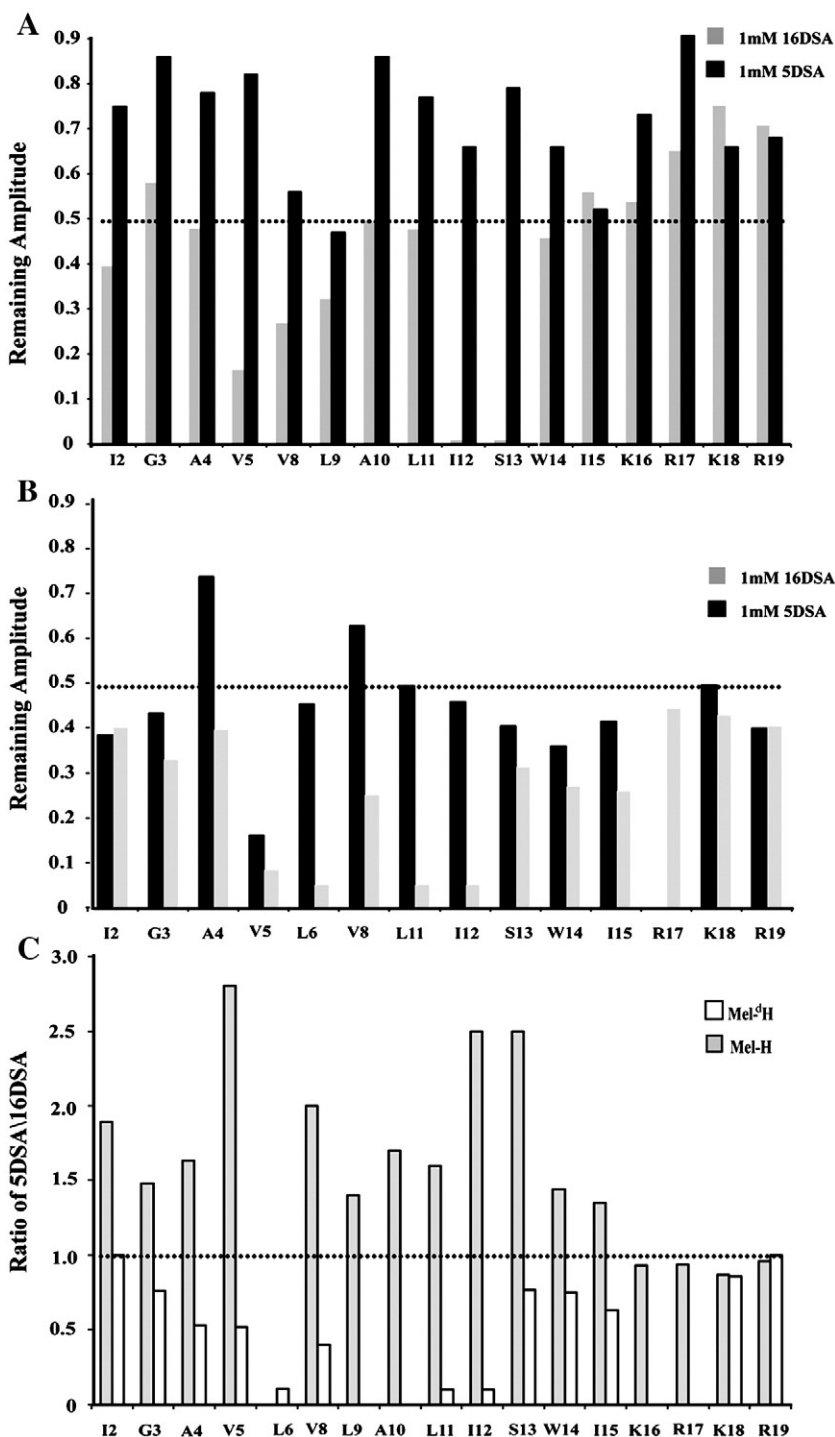


**Fig. 8.** Bar diagram showing resonance perturbation of micelle-bound Mel-H (panel A) and Mel-dH (panel B) with spin labeled lipids 5-doxyl-stearic acid (5-DOSA) and 16-doxyl-stearic acid (16-DOSA). 5-DOSA perturbs amino acids at the surface and 16-DOSA perturbs those at the interior of the lipid micelles. The C $\alpha$ H/NH cross peaks signal intensity were estimated from 2D- $^1\text{H}$ - $^1\text{H}$  TOCSY spectrum of DPC micelle-bound peptides at 310 K at a various concentrations of spin labeled lipids. (panel C) A bar diagram showing ratio of perturbation in 5-DOSA and 16-DOSA for Mel-H and Mel-dH peptides. A ratio of >1 clearly indicates corresponding residue to be perturbed predominantly by 16-DOSA, indicating a deeper penetration of the residue into the non-polar environment of micelles.

DPC strongly indicates that the peptide is more mobile or dynamic in the lipid micelles.

#### 4. Discussion

Helical AMPs constitutes a large pool of host defense molecules in every living organism [2,3]. Three-dimensional structures of many of these AMPs show a tendency to adopt a bend or kinked conforma-

tions in lipid micelles [34,50,51]. The functional and structural consequences of these helix interrupting sequences are not clearly understood. Melittin is arguably the most well studied membrane-lytic amphipathic helical peptide. Three-dimensional structure of melittin is characterized by a central bend that orients two helical segments, at the N- and C-termini, into a defined angle [43–46]. The hinge region of melittin including the residue P14 has been implicated into lipid interactions, membrane orientation, hemolytic acti-

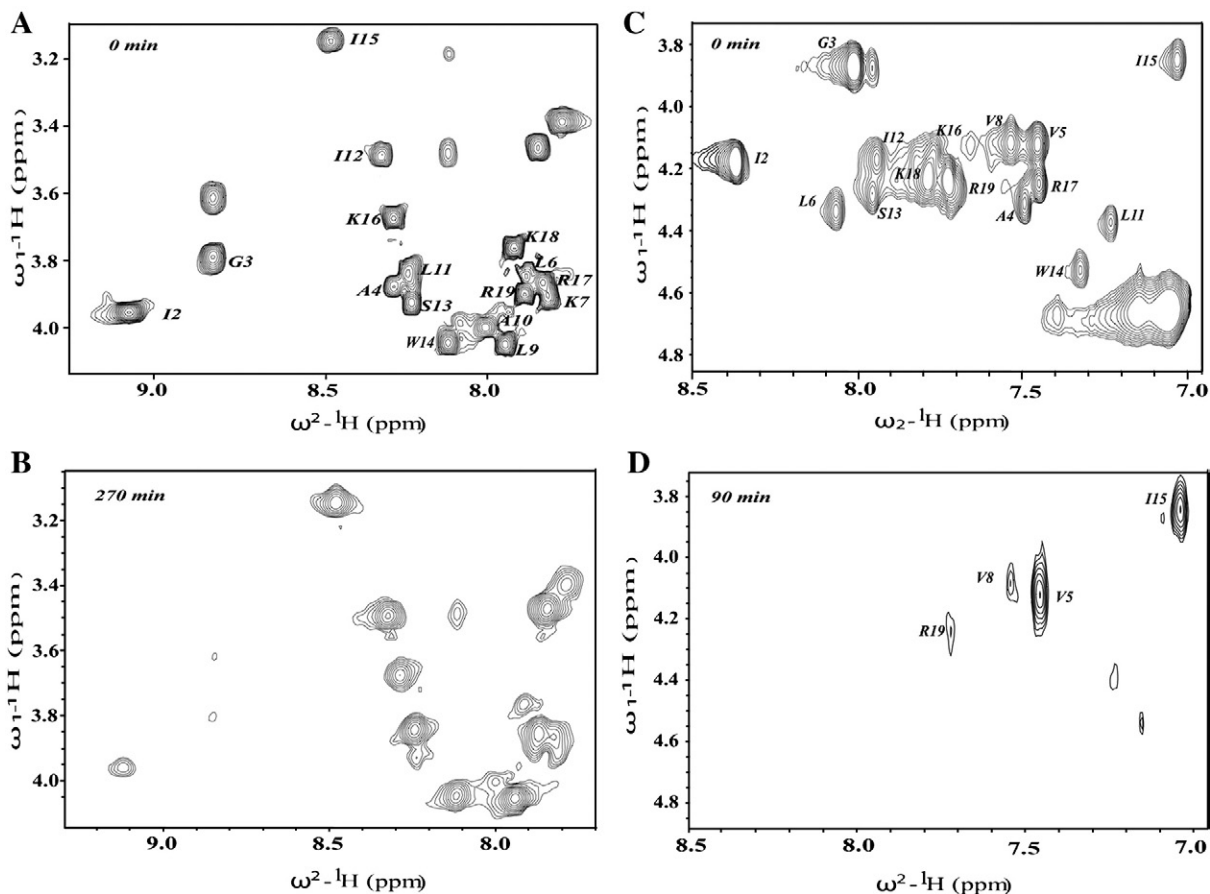


**Fig. 9.** Two-dimensional  $^1\text{H}$ - $^1\text{H}$  TOCSY spectra of micelle-bound Mel-H and Mel- $^d\text{H}$ , obtained in  $\text{D}_2\text{O}$ , showing slowly exchanging  $\text{C}\alpha\text{H}/\text{NH}$  cross peaks. H-D exchange behavior of Mel-H in a freshly dissolved sample (panel A) and after 270 min exchange (panel B). H-D exchange behavior of Mel- $^d\text{H}$  of a freshly dissolved sample (panel C) and after 90 min exchange (panel D). NMR experiments were carried out at pH 3, 310 K.

vity and channel formation [60–62]. The single residue deletion studies of melittin had demonstrated that deletion of Leu from the TTGLP sequence had caused significant reduction of the both activities, antibacterial and hemolytic, of melittin [27]. Interestingly, replacement of Pro14 in the hinge region with Ala had been found to enhance the hemolytic activity of melittin [60] and altered its self-aggregations, membrane binding and pore forming kinetics [61,62]. Incorporation of four D-amino acids,  $^d\text{V5}$ ,  $^d\text{V8}$ ,  $^d\text{I17}$  and  $^d\text{K21}$ , into the native melittin (26-residue) had yielded a low hemolytic peptide containing antimicrobial activities [36]. Binding studies of melittin and its diastereomer with different lipids showed that a low affinity

binding of the diastereomer with the zwitterionic lipid vesicles [36,37]. A Surface Plasmon Resonance (SPR) study had determined kinetics of interactions of melittin and the diastereomer ( $^d\text{V5}$ ,  $^d\text{V8}$ ,  $^d\text{I17}$  and  $^d\text{K21}$ ) with PC/cholesterol and PG/PE monolayers and bilayers [38]. The authors had suggested that the poor hemolytic property of the 26-residue diastereomeric form of melittin is related to the inability of the peptide to insert into the inner layer of the lipid vesicles [38]. An NMR structure of the diastereomer obtained in a mixed lipid micelles (DPC/DMPG, 4:1) demonstrated a helical structure at the C-terminus and a highly flexible conformations for the N-terminus region [39].

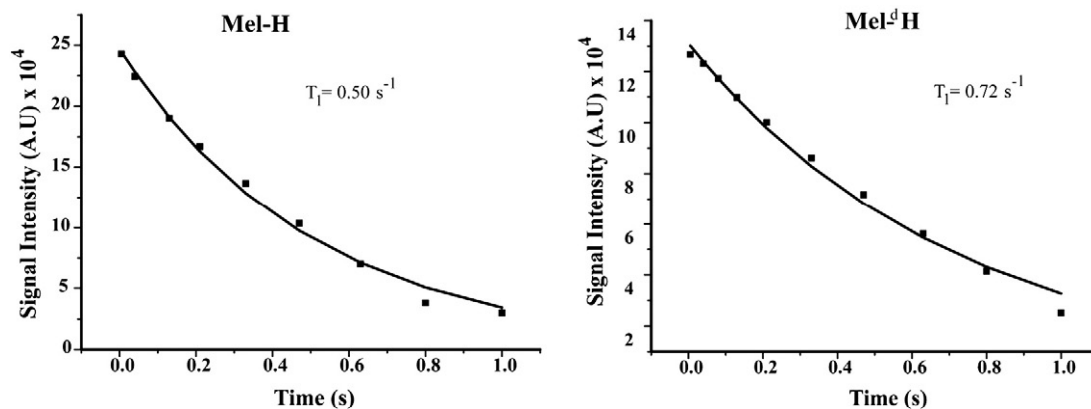


**Fig. 10.** The proton longitudinal relaxation ( $T_1$ ) measurement of deuterated DPC micelle-bound Mel-H (left) and Mel- $^d\text{H}$  (right).  $T_1$  values were estimated by fitting the signal intensity of an upfield shifted methyl resonance at 0.86 ppm belonging to residue Leu11 from 1-D proton NMR spectra obtained at 310 K, as a function of relaxation delays.

In this work, we demonstrate that deletion of the hinge region of melittin, yielding a ~19 residue peptide, does not affect its antibacterial activity, although the high hemolytic activity of melittin has been found to be reduced (Table 1). The diastereomeric analog, Mel-<sup>d</sup>H, containing D-amino acids [<sup>d</sup>V5, <sup>d</sup>V8, <sup>d</sup>L11, <sup>d</sup>K16], possesses antimicrobial activities, however, the hemolytic activity has been drastically reduced. Incorporation of D-amino acids into antimicrobial peptide sequences could be an attractive approach to develop cell selective antimicrobial peptides. Such inclusion had often resulted in disruption of hemolytic or cytotoxic properties of lytic peptides without the expense of antimicrobial activities, including melittin, pardaxin and gramicidin S [36,40–42]. However, the cell selective behavior of these diastereomeric forms is not easily understood. Here, we have utilized Mel-M and Mel-<sup>d</sup>H as a model system to elucidate structural and dynamical aspects, obtained from DPC micelles, of selective cell lysis. We have estimated binding affinities of Mel-H and Mel-<sup>d</sup>H with DPC micelles using ITC. It appears that Mel-H binds to DPC micelles with slightly higher affinity as compared to the Mel-<sup>d</sup>H (Table 2). The lipid/peptide interactions are enthalpy driven indicating ionic or hydrogen bond formation could be dominant in stabilizing the complexes. In parallel with ITC, the NMR pulse-field-gradient studies demonstrate that Mel-H and Mel-<sup>d</sup>H both are equally well partitioned into the zwitterionic lipid micelles (Fig. 2). In complex with DPC micelles, Mel-H adopts a well defined helical structure without any evidence for kink or bend. Helical structures of antimicrobial peptides obtained in lipid micelles are often characterized by bends. Micelle curvature has been thought to be responsible for such distortion. The straight helical structure of Mel-H in DPC micelles indicates that micelle curvature may not be an important factor in inducing structural kink. The one face of the Mel-H helix is highly non-polar due to the presence of array of hydrophobic residues I2, V5, V8, L9, I12 and I15. The other face of the helix is of mixed polarity containing non-polar residues L6, A10, L11 and W14 with three positively charged residues K7, R17 and K18 (Fig. 7). The residue W14 shows an interesting packing arrangement, whereby the aromatic sidechain is sandwiched between residues L11 and K18, demonstrating non-polar and cation- $\pi$  type interactions in the formation of the helical conformation (Fig. 7). DPC-bound structure of Mel-<sup>d</sup>H peptide is found to be rather compact despite the disruption of canonical helical structure due to the incorporation of several D-amino acids into the sequence (Fig. 7). The N-terminus of Mel-<sup>d</sup>H is stabilized by multiple  $\beta$ -turn conformations with a short helix at the C-terminus (Fig. 7). The non-polar sidechains of residues I2, V5, L9, A10, L11 and W14 reside in one face of the structure (Fig. 7). The four cationic residues, KRKR, at the C-terminus are largely disordered. The inter-sidechain interactions in the Mel-<sup>d</sup>H structure have significantly been reduced. Since, there was less number of NOE contacts among the sidechains (Table 3). In particular the cation- $\pi$  type packing between residues W14/K18 was absent in the case of Mel-<sup>d</sup>H. Therefore, our results demonstrate that Mel-<sup>d</sup>H acquires a folded backbone conformation in zwitterionic DPC micelles but the interactions among the sidechains are rather limited in the structure. We envision that these conformational differences between Mel-H and Mel-<sup>d</sup>H may be reflected into dynamics and micelle localization of the peptides. We have utilized H-D exchange and proton  $T_1$  relaxation measurements to describe the dynamics of Mel-H and Mel-<sup>d</sup>H. H-D exchange studies in DPC micelles reveal that amide protons of Mel-<sup>d</sup>H undergo a significantly fast exchange with D<sub>2</sub>O (Fig. 9). On the other hand, the amide protons of Mel-H peptide show a marked slow exchange behavior. These data can be explained by a surface localization of Mel-<sup>d</sup>H in micelles and/or intrinsic flexibility in the DPC-bound state of the peptide. The higher  $T_1$  values of Mel-<sup>d</sup>H peptide demonstrate that a conformational flexibility in DPC micelles (Fig. 10). By contrast, the micelle-bound state of Mel-H peptide is appeared to be much rigid with less conformational freedom as suggested by the slow amide exchange and shorter  $T_1$  values of

protons (Figs. 9 and 10). The micelle localization experiments probed by the two paramagnetic doxyl lipids clearly show Mel-H is inserted deeper into micelle whereas Mel-<sup>d</sup>H is anchored at the surface as evidence by a larger perturbation of Mel-H and Mel-<sup>d</sup>H by 16-DSA and 5-DSA, respectively (Fig. 8). These results provide new insights into the molecular mechanisms of hemolytic activities of diastereomeric peptides. Although, Mel-H and Mel-<sup>d</sup>H binds to lipid micelles adopting folded amphipathic structures, it is likely that a larger dynamics and surface localization of the Mel-<sup>d</sup>H peptide in zwitterionic micelles may be responsible for the limited or low hemolytic property. Such dynamic nature of the structure in lipid complex might prevent a better penetration of the diastereomeric peptide into the cell membrane that is essential for lytic activity. It is worthy to mention that the micelle-bound structures and dynamics of membrane active peptides may have to be validated by further investigations using lipid bilayers. Thus, combined structural and dynamical information obtained from lipid micelles and bilayer systems would be undoubtedly helpful for better understanding of the molecular mechanism of cell selective activity of antimicrobial peptides.

### Acknowledgement

This work is funded by A\*BMRC, Singapore (06/01/22/19/446).

### Appendix A. Supplementary data

Supplementary data associated with this article can be found, in the online version, at doi:10.1016/j.bbamem.2009.07.014.

### References

- [1] H.G. Boman, Peptide antibiotics and their role in innate immunity, *Annu. Rev. Immunol.* 13 (1995) 61–92.
- [2] I. Zelezetsky, A. Tossi, Alpha-helical antimicrobial peptides—using a sequence template to guide structure-activity relationship studies, *Biochim. Biophys. Acta* 1758 (2006) 1436–1449.
- [3] R.M. Epanand, H.J. Vogel, Diversity of antimicrobial peptides and their mechanisms of action, *Biochim. Biophys. Acta* 1462 (1999) 11–28.
- [4] R.E. Hancock, Cationic peptides: effectors in innate immunity and novel antimicrobials, *Lancet Infect. Dis.* 1 (2001) 156–164.
- [5] M. Zasloff, Antimicrobial peptides of multicellular organisms, *Nature* 415 (2002) 389–395.
- [6] U. Dürr, U.S. Sudheendra, A. Ramamoorthy, LL-37, the only human member of the cathelicidin family of antimicrobial peptides, *Biochim. Biophys. Acta* 1758 (2006) 1408–1425.
- [7] V. Dhople, A. Krukemeyer, A. Ramamoorthy, The human beta-defensin-3, an antibacterial peptide with multiple biological functions, *Biochim. Biophys. Acta* 1758 (2006) 1499–1512.
- [8] B. Bechinger, K. Lohner, Detergent-like actions of linear amphipathic cationic antimicrobial peptides, *Biochim. Biophys. Acta* 1758 (2006) 1529–1539.
- [9] H. Sato, J.B. Feix, Peptide-membrane interactions and mechanisms of membrane destruction by amphipathic alpha-helical antimicrobial peptides, *Biochim. Biophys. Acta* 1758 (2006) 1245–1256.
- [10] A. Ramamoorthy, Beyond NMR spectra of antimicrobial peptides: dynamical images at atomic resolution and functional insights, *Solid State Nucl. Magn. Reson.* 35 (4) (2009) 201–207.
- [11] A. Ramamoorthy, D. Lee, J.S. Santos, K.A. Henzler-Wildman, Nitrogen-14 solid-state NMR spectroscopy of aligned phospholipid bilayers to probe peptide–lipid interaction and oligomerization of membrane associated peptides, *J. Am. Chem. Soc.* 130 (2008) 11023–11029.
- [12] A. Tossi, L. Sandri, A. Giangaspero, Amphipathic, alpha-helical antimicrobial peptides, *Biopolymers* 55 (2000) 4–30.
- [13] H. Jenssen, P. Hamill, R.E. Hancock, Peptide antimicrobial agents, *Clin. Microbiol. Rev.* 19 (2006) 491–511.
- [14] Y. Shai, Mode of action of membrane active antimicrobial peptides, *Biopolymers* 66 (2002) 236–248.
- [15] L.M. Gottler, A. Ramamoorthy, Structure, membrane orientation, mechanism, and function of pexiganan—a highly potent antimicrobial peptide designed from magainin, *Biochim. Biophys. Acta* 1788 (8) (2009) 1680–1686.
- [16] S.E. Blondelle, K. Lohner, Combinatorial libraries: a tool to design antimicrobial and antifungal peptide analogues having lytic specificities for structure–activity relationship studies, *Biopolymers* 55 (2000) 74–87.
- [17] J.E. Oh, S.Y. Hong, K.H. Lee, Structure–activity relationship study: short antimicrobial peptides, *J. Pept. Res.* 53 (1999) 41–46.
- [18] N. Sitaram, R. Nagaraj, Interaction of antimicrobial peptides with biological and model membranes: structural and charge requirements for activity, *Biochim. Biophys. Acta* 1462 (1999) 29–54.

- [19] E. Habermann, Bee and wasp venoms, *Science* 177 (1972) 314–322.
- [20] H. Raghuraman, A. Chattopadhyay, Melittin: a membrane-active peptide with diverse functions, *Biosci. Rep.* 27 (2007) 189–223.
- [21] C.E. Dempsey, The actions of melittin on membranes, *Biochim. Biophys. Acta* 1031 (1990) 143–161.
- [22] K. Matsuzaki, S. Yoneyama, K. Miyajima, Pore formation and translocation of melittin, *Biophys. J.* 73 (1997) 831–838.
- [23] S. Rex, G. Schwarz, Quantitative studies on the melittin-induced leakage mechanism of lipid vesicles, *Biochemistry* 37 (1998) 2336–2345.
- [24] M.T. Lee, W.C. Hung, F.Y. Chen, H.W. Huang, Mechanism and kinetics of pore formation in membranes by water-soluble amphipathic peptides, *Proc. Natl. Acad. Sci. U. S. A.* 105 (2008) 5087–5092.
- [25] G. van den Bogaart, J.V. Guzman, J.T. Mika, B. Poolman, On the mechanism of pore formation by melittin, *J. Biol. Chem.* 283 (2008) 33854–33857.
- [26] A.S. Ladokhin, S.H. White, Folding of amphipathic alpha-helices on membranes: energetics of helix formation by melittin, *J. Mol. Biol.* 285 (1999) 1363–1369.
- [27] S.E. Blondelle, R.A. Houghten, Hemolytic and antimicrobial activities of the twenty-four individual omission analogues of melittin, *Biochemistry* 30 (1991) 4671–4678.
- [28] S.E. Blondelle, L.R. Simpkins, E. Perez-Paya, R.A. Houghten, Influence of tryptophan residues on melittin's hemolytic activity, *Biochim. Biophys. Acta* 1202 (1993) 331–336.
- [29] C. Subbalakshmi, R. Nagaraj, N. Sitaram, Biological activities of C-terminal 15-residue synthetic fragment of melittin: design of an analog with improved antibacterial activity, *FEBS Lett.* 448 (1999) 62–66.
- [30] N. Asthana, S.P. Yadav, J.K. Ghosh, Dissection of antibacterial and toxic activity of melittin: a leucine zipper motif plays a crucial role in determining its hemolytic activity but not antibacterial activity, *J. Biol. Chem.* 279 (2004) 55042–55050.
- [31] W.L. Zhu, Y.M. Song, Y. Park, K.H. Park, S.T. Yang, J.I. Kim, I.S. Park, K.S. Hahn, S.Y. Shin, Substitution of the leucine zipper sequence in melittin with peptidic residues affects self-association, cell selectivity, and mode of action, *Biochim. Biophys. Acta* 1768 (2007) 1506–1517.
- [32] H.G. Boman, D. Wade, I.A. Boman, B. Wahlin, R.B. Merrifield, Antibacterial and antimalarial properties of peptides that are cecropin-melittin hybrids, *FEBS Lett.* 259 (1989) 103–106.
- [33] C. Friedrich, M.G. Scott, N. Karunaratne, H. Yan, R.E. Hancock, Salt-resistant alpha-helical cationic antimicrobial peptides, *Antimicrob. Agents. Chemother.* 43 (1999) 1542–1548.
- [34] F. Porcelli, B.A. Buck-Koehntop, S. Thennarasu, A. Ramamoorthy, G. Veglia, Structures of the dimeric and monomeric variants of magainin antimicrobial peptides (MSI-78 and MSI-594) in micelles and bilayers, determined by NMR spectroscopy, *Biochemistry* 45 (2006) 5793–5799.
- [35] A. Ramamoorthy, S. Thennarasu, D.K. Lee, A. Tan, L. Maloy, Solid-state NMR investigation of the membrane-disrupting mechanism of antimicrobial peptides MSI-78 and MSI-594 derived from magainin 2 and melittin, *Biophys. J.* 91 (2006) 206–216.
- [36] Z. Oren, J. Hong, Y. Shai, A repertoire of novel antibacterial diastereomeric peptides with selective cytolytic activity, *J. Biol. Chem.* 272 (1997) 14643–14649.
- [37] Z. Oren, Y. Shai, Selective lysis of bacteria but not mammalian cells by diastereomers of melittin: structure–function study, *Biochemistry* 36 (1997) 1826–1835.
- [38] N. Papo, Y. Shai, Exploring peptide membrane interaction using surface plasmon resonance: differentiation between pore formation versus membrane disruption by lytic peptides, *Biochemistry* 42 (2003) 458–466.
- [39] M. Sharon, Z. Oren, Y. Shai, J. Anglister, 2D-NMR and ATR-FTIR study of the structure of a cell-selective diastereomer of melittin and its orientation in phospholipids, *Biochemistry* 38 (1999) 15305–15316.
- [40] L.H. Kondejewski, M. Jelokhani-Niaraki, S.W. Farmer, B. Lix, C.M. Kay, B.D. Sykes, R. E. Hancock, R.S. Hodges, Dissociation of antimicrobial and hemolytic activities in cyclic peptide diastereomers by systematic alterations in amphipathicity, *J. Biol. Chem.* 274 (1999) 13181–13192.
- [41] Y. Shai, Z. Oren, Diastereoisomers of cytolysins, a novel class of potent antibacterial peptides, *J. Biol. Chem.* 271 (1996) 7305–7308.
- [42] G. Wang, Determination of solution structure and lipid micelle location of an engineered membrane peptide by using one NMR experiment and one sample, *Biochim. Biophys. Acta* 1768 (2007) 3271–3281.
- [43] T.C. Terwilliger, D. Eisenberg, The structure of melittin. I. Structure determination and partial refinement, *J. Biol. Chem.* 257 (1982) 6010–6015.
- [44] F. Inagaki, I. Shimada, K. Kawaguchi, M. Hirano, I. Terasawa, T. Ikura, N. Go, Structure of melittin bound to perdeuterated dodecylphosphocholine micelles as studied by two-dimensional NMR and distance geometry calculations, *Biochemistry* 28 (1989) 5985–5991.
- [45] B. Bechinger, The structure, dynamics and orientation of antimicrobial peptides in membranes by multidimensional solid-state NMR spectroscopy, *Biochim. Biophys. Acta* 1462 (1999) 157–183.
- [46] A. Naito, T. Nagao, K. Norisada, T. Mizuno, S. Tuzi, H. Saito, Conformation and dynamics of melittin bound to magnetically orientated lipid bilayers by solid-state  $^{31}\text{P}$  and  $^{13}\text{C}$  NMR spectroscopy, *Biophys. J.* 78 (2000) 2405–2417.
- [47] R. Bazzo, M.J. Tappin, A. Pastore, T.S. Harvey, J.A. Carver, I.D. Campbell, The structure of melittin. A  $^1\text{H}$ -NMR study in methanol, *Eur. J. Biochem.* 173 (1988) 139–146.
- [48] S. Bhattacharjya, J. Venkatraman, A. Kumar, P. Balam, Fluoroalcohols as structure modifiers in peptides and proteins: hexafluoroacetone hydrate stabilizes a helical conformation of melittin at low pH, *J. Pept. Res.* 54 (1999) 100–111.
- [49] A. Bhunia, P.N. Domadia, S. Bhattacharjya, Structural and thermodynamic analyses of the interaction between melittin and lipopolysaccharide, *Biochim. Biophys. Acta* 1768 (2007) 3282–3291.
- [50] F. Porcelli, B. Buck, D.K. Lee, K.J. Hallock, A. Ramamoorthy, G. Veglia, Structure and orientation of pardaxin determined by NMR experiments in model membranes, *J. Biol. Chem.* 279 (2004) 45815–45823.
- [51] F. Porcelli, R. Verardi, L. Shi, K.A. Henzler-Wildman, A. Ramamoorthy, G. Veglia, NMR structure of the cathelicidin-derived human antimicrobial peptide LL-37 in dodecylphosphocholine micelles, *Biochemistry* 47 (2008) 5565–5572.
- [52] N.J. Traaseth, R. Verardi, K.D. Torgersen, C.B. Karim, D.D. Thomas, G. Veglia, Spectroscopic validation of the pentameric structure of phospholamban, *Proc. Natl. Acad. Sci. U. S. A.* 104 (2007) 14676–14681.
- [53] R. Ferre, E. Badosa, L. Feliu, M. Planas, E. Montesinos, E. Bardaji, Inhibition of plant-pathogenic bacteria by short synthetic cecropin A-melittin hybrid peptides, *Appl. Environ. Microbiol.* 72 (2006) 3302–3308.
- [54] A. Bhunia, P.N. Domadia, H. Mohanram, S. Bhattacharjya, NMR structural studies of the Ste11 SAM domain in the dodecyl phosphocholine micelle, *Proteins* 74 (2009) 328–343.
- [55] S. Bhattacharjya, P. Xu, H. Xiang, M. Chretien, N.G. Seidah, F. Ni, pH-induced conformational transitions of a molten-globule-like state of the inhibitory prodomain of furin: implications for zymogen activation, *Protein Sci.* 10 (2001) 934–942.
- [56] P. Guntert, C. Mumenthaler, K. Wuthrich, Torsion angle dynamics for NMR structure calculation with the new program DYANA, *J. Mol. Biol.* 273 (1997) 283–298.
- [57] G. Cornilescu, F. Delaglio, A. Bax, Protein backbone angle restraints from searching a database for chemical shift and sequence homology, *J. Biomol. NMR* 13 (1999) 289–302.
- [58] K. Wuthrich, NMR of proteins and nucleic acids (1986).
- [59] D.S. Wishart, B.D. Sykes, F.M. Richards, Relationship between nuclear magnetic resonance chemical shift and protein secondary structure, *J. Mol. Biol.* 222 (1991) 311–333.
- [60] C.E. Dempsey, R. Bazzo, T.S. Harvey, I. Syperek, G. Boheim, I.D. Campbell, Contribution of proline-14 to the structure and actions of melittin, *FEBS Lett.* 281 (1991) 240–244.
- [61] C.E. Dempsey, B. Sternberg, Reversible disc-micellization of dimyristoylphosphatidylcholine bilayers induced by melittin and [Ala-14]melittin, *Biochim. Biophys. Acta* 1061 (1991) 175–184.
- [62] S. Rex, A Pro→Ala substitution in melittin affects self-association, membrane binding and pore-formation kinetics due to changes in structural and electrostatic properties, *Biophys. Chem.* 85 (2000) 209–228.